Scientific Reports

https://doi.org/10.1038/s41598-026-35012-8

Article in Press

Both emissions and ageing altered brown carbon aerosols in the East Asian outflow

Received: 3 October 2025

Accepted: 1 January 2026

Published online: 06 January 2026

Cite this article as: Zhu C., Miyakawa T., Taketani F. *et al.* Both emissions and ageing altered brown carbon aerosols in the East Asian outflow. *Sci Rep* (2026). https://doi.org/10.1038/s41598-026-35012-8

Chunmao Zhu, Takuma Miyakawa, Fumikazu Taketani, Bhagawati Kunwar, Dhananjay Kumar, Kimitaka Kawamura & Yugo Kanaya

Both emissions and ageing altered brown carbon aerosols in the East Asian outflow

Chunmao Zhu[1], Takuma Miyakawa[1], Fumikazu Taketani[1], Bhagawati Kunwar[2†], Dhananjay Kumar Deshmukh[2††], Kimitaka Kawamura[2], Yugo Kanaya[1]*

[1]Research Institute for Global Change, Japan Agency for Marine-Earth Science and Technology (JAMSTEC), Yokohama 2360001, Japan

[2]Chubu Institute for Advanced Studies, Chubu University, Kasugai 4878501, Japan

*Corresponding author: Chunmao Zhu (chmzhu@jamstec.go.jp)

ABSTRACT: Brown carbon aerosols (BrC) significantly contribute to regional climate warming in East Asia. However, their sources and atmospheric transformation remain poorly constrained due to limited observations. In this study, we clarified the seasonal dynamics of BrC and quantified the sources of relating carbonaceous components, at the gateway of the East Asian air outflow for seasonal variations. Our findings reveal that fossil fuel combustion dominates the sources of BrC containing carbonaceous components in winter, while biomass burning and local biogenic sources become more prominent in spring and summer, respectively. We provide benchmark optical properties of BrC for climate model simulations, demonstrating that the absorption coefficient and mass absorption cross-section of water-soluble fraction from land-originated air masses (0.47 Mm^{-1} and 0.53 $m^2\ gC^{-1}$, respectively) are more than twice those of sea-originated air masses (0.11 Mm^{-1} and 0.21 $m^2\ gC^{-1}$, respectively). Additionally, we show that BrC undergoes photochemical degradation during transport with a half-life of approximately 1.2 days. A significant reduction in BrC levels during the COVID-19 lockdown period highlights the potential of stringent emission controls to mitigate air pollution and its associated climate impacts. By shedding light on the seasonal dynamics, diverse sources, and atmospheric ageing of BrC, the study provides valuable insights for emission reduction strategies and improving BrC representation in climate models.

KEYWORDS: Brown carbon aerosols; Light-absorption properties; Molecular tracers; Radiocarbon; Fossil fuel combustion; Biomass burning; East Asian outflow

SYNOPSIS: Sources and atmospheric transformation of brown carbon aerosols are less studied. This work clarified the effects of varying seasonal sources and ageing processes on brown carbon aerosols, providing benchmark optical properties for climate models.

1. INTRODUCTION

Brown carbon aerosols (BrC) are an important yet poorly understood component of atmospheric aerosols that contribute significantly to global warming through the absorption of visible and ultraviolet light.[1-4] BrC accounts for approximately one-quarter of the radiative forcing by carbonaceous aerosols, with a global radiative forcing range of 0.1–0.6 W m^{-2}.[5-7] While legislative efforts to reduce anthropogenic emissions have been implemented globally,[8-12] the radiative influence of carbonaceous aerosols, including BrC, has paradoxically increased over the past two decades.[13] This trend suggests that BrC's warming potential is underestimated in current radiative transfer models, which are crucial for predicting future climate scenarios.[14-17]

The optical properties of BrC vary substantially by region and season, influenced by differences in source composition, atmospheric condition, and

photochemical ageing processes.[17-21] Fossil fuel combustion and biomass burning are recognized as dominant sources of BrC,[22-24] but secondary BrC formation from atmospheric reactions is increasingly relevant, particularly in densely populated cities in the lower-latitude northern hemisphere, often relating to photoenhancement.[20,25,26] Photochemical degradation, or photobleaching, further complicates BrC's climatic effects, as the rate of optical decay depends on complex atmospheric conditions.[18,27-29]

East Asia, a region characterized by intense anthropogenic activity, is a major source of BrC aerosols. Emission control policies in China, such as the Action Plan on the Prevention and Control of Air Pollution, have significantly reduced carbonaceous aerosol emissions since 2010.[30-32] However, these reductions are partially offset by contributions from biogenic sources and secondary BrC formation.[33,34] Additional sources, such as crop residue burning in China and forest fires in Russia,[35,36] further complicate the BrC budget. The anticipated increase in wildfires in Asia under future climate scenarios underscore the urgent need to quantify the temporal variability and source-specific contributions of BrC in this region.[35,37]

While recent observational studies have characterized BrC in urban and industrial zones,[21, 29, 38] there is still limited data on BrC properties in the East Asian outflow region,[4] where aerosols undergo long-range transport and atmospheric transformation before impacting regional and global climate.[18,19,29] Addressing this gap, this study focuses on BrC aerosols at

Fukue Island, a remote site in Japan situated at the gateway of the East Asian outflow. By combining optical measurements, molecular tracers, atmospheric transport model and radiocarbon analysis, we aim to: (1) Characterize the seasonal variations in BrC light-absorption properties; (2) Investigate the effects of atmospheric transport and photochemical ageing on BrC; (3) Quantify the source contributions to BrC containing carbonaceous components; and (4) Provide recommendations for incorporating BrC dynamics into climate models. Water-soluble BrC fraction was targeted for (2) to compare with previous studies. Through these analyses, this study seeks to enhance our understanding of BrC processes in the East Asian outflow and their implications for regional and global climate.

2. MATERIALS AND METHODS

2.1 Observation site and sample collection

Observations were conducted at the Fukue Atmospheric Environment Observatory (32.75° N, 128.68° E, 80 m above sea level) on Fukue Island (326.43 km^2), a remote site in western Japan. The observatory, located on the northwestern rim of the island and approximately 23 km from the main town, minimizes the influence of local anthropogenic emissions. $PM_{2.5}$ samples were collected between November 2019 and November 2020 at 5-day intervals on the rooftop of the observatory (~3.5 m above ground level). Aerosol particles were collected using a high-volume air sampler (Model 120SL, Kimoto Electric Ltd., Osaka, Japan) equipped with a single-stage

cascade impactor (TE-231, Tisch Environmental Inc., Cleves, Ohio, USA). The $PM_{2.5}$ fraction was captured on quartz fiber filters (2500QAT-UP, 8 inch × 10 inch, Cytiva, Washington D.C., USA) under an airflow rate of 1.13 m^3 min^{-1}, while coarse particles (> 2.5 μm) were removed using stripped filters (TE-230QZ, Tisch Environmental Inc., Cleves, Ohio, USA). Filters were preheated at 900 °C for 3 hours before use and stored at –20 °C after collection to prevent contamination and degradation. Field blanks, collected every 2 months following the same procedures without operating the sampler pump, were used for quality control. A total of 71 samples and 6 field blanks were collected.

2.2 Quantification of carbonaceous components

Total carbon (TC), including elemental carbon (EC) and organic carbon (OC), were quantified using a thermal-optical transmittance method with a carbon analyzer (Sunset Laboratory Inc., USA),[39] following the Interagency Monitoring Protected Visual Environments thermal evolution protocol. The analytical error in replicate analyses was within 8%. Sample data were corrected for field blanks, which contained OC levels of < 5% of the samples. Water soluble organic carbon (WSOC) was measured using a carbon/nitrogen analyzer (TOC–V_{CSH}, Shimadzu Corp., Kyoto, Japan). Methanol-soluble organic carbon (MSOC) was determined to evaluate BrC that including both water-soluble and water-insoluble components. A portion of the aerosol filter (5.5 cm × 4.45 cm) was extracted with 20 ml of methanol under static

conditions for 30 minutes, followed by drying in a well-ventilated clean draft for 2 hours. The residue, methanol insoluble organic carbon (MIOC), was analyzed using the same carbon analyzer. MSOC was calculated as the difference between OC and MIOC. To investigate the uncertainty, we compared MIOC and OC for 6 field blank filters collected spanning the study period (November 14, 2019, January 13, 2020, March 23, 2020, June 12, 2020, August 16, 2020, and October 15, 2020). The mean MIOC was quantified as 0.0065 ± 0.0012 μg m^{-3}, assuming a mean samplig air volume of 8000 m^3 , which is close to the real condition. This MIOC level was much lower than the mean total OC of 0.1243 ± 0.0618 μg m^{-3} for the same field blanks. Such results indicated that there is negligible methanol remaining in the filter after 2 hour drying.

2.3 Light absorption analyses

BrC light absorption was analyzed using both water and methanol extracts due to ongoing debates regarding solvent efficiency.[5,40,41] Methanol is known to extract BrC more effectively, but may overestimate absorption due to significant extinction caused by suspended insoluble particles in the extracts, a phenomenon not observed in water extracts.[42] Meanwhile, methanol can extract more light-absorbing chromophores, but also includes water-soluble compounds, potentially leading to overlap between the fractions. In this study, methanol and water extractions were performed on separate filter punches to preserve sample integrity for different analyses, rather than using

a sequential extraction approach (water followed by methanol). While this limits full isolation of water-insoluble BrC, it avoids potential cross-contamination during sequential extractions. For comparison, water-based results were emphasized to align with previous studies. Filter sections (2 cm^2) were extracted in 40 ml of ultrapure water or methanol under ultrasonication for 15 min, with intermittent manual shaking. Extracts were filtered through 0.20 µm syringe filters (Millex-LG for water extraction and Millex-FG for methanol extraction, Merck KGaA, Darmstadt, Germany). This filtration could remove most suspended insoluble particles, including black carbon (BC), which may cause overestimated absorption as described above. With this protocol, we confirmed that the light absorption by BC was negligible as shown by the relationship with BC concentration beyond 700 nm (Fig. S1).

Absorption spectra were measured using a spectrophotometer (U-2910, Hitachi Inc., Tokyo, Japan) over 210–880 nm at 1 nm resolution. Absorption coefficients (Abs) were calculated from liquid-phase absorption and the sampled air volume (8000–8500 m^3).[43] Abs at 365 nm (Abs_{365}, mean value of 361–370 nm) was used as a representative metric for BrC light-absorption. The absorption Angstrom exponent (AAE), quantifying wavelength dependency, was determined from the slope of Ln (Abs) versus Ln (□) over 340–500 nm. The mass absorption cross-section (MAC), representing light absorption per unit mass of BrC, was calculated as the ratio of Abs_{365} with the OC mass extracted with water ($MAC_{365\text{-}WSOC}$) or methanol ($MAC_{365\text{-}MSOC}$).

2.4 Estimation of photobleaching rate

Photobleaching rate of BrC was quantified by fitting $MAC_{365\text{-}WSOC}$ as a function of atmospheric transport time using the equation:[18,44]

$$MAC_{365\text{-}WSOC} = a + b \cdot e^{-kt} \quad (1)$$

where k is the first-order photobleaching rate (day^{-1}), t (day) is the mean transport time (days) from the Asian continent to Fukue. Although BrC is not always exposed to light during transport, t is a good index to show the potential of light exposure for the ambient atmosphere. a represents the regional background MAC, and b is the initial MAC before transport. Transport times were estimated using the Hybrid Single-Particle Lagrangian Integrated Trajectory (HYSPLIT) model,[45] and half-life was calculated as Ln (2)/k. The model was applied separately for China-dominated and all land-origin footprints.

2.5 Molecular tracer analysis

Organic tracers were analyzed using gas chromatography/mass spectrometry (GC/MS).[46-49] Briefly, filter sections (~ 10 cm^2) were extracted three times with dichloromethane/methanol (2:1, v/v) under ultrasonication. Extracts were concentrated, derivatized with N, O-bis-(trimethylsilyl) trifluoroacetamide, and quantified using an Agilent 7890A GC equipped with an HP-5 ms capillary column (30 m × 0.25 mm × 0.25 mm) and an Agilent 5975C mass-selective detector. Mass concentrations of organic compounds

were determined by comparing the response of the peak area relative to those of the authentic standards. Internal standards ensured recoveries > 80%, and analytical errors < 15%. No peak for the reported organic compounds was found in the field and laboratory blanks.

2.6 Source apportionment via PMF

Source contributions to WSOC throughout the year were assessed using the Positive Matrix Factorization (PMF) model (version 5.0).[50] The attributed sources were then investigated for the relations with BrC light absorption. Input variables included 21 organic tracers, 3 carbonaceous components (WSOC, WIOC and EC), and 8 water-soluble ions (Fig. S2). OC was designated as the total variable for PMF simulation, with uncertainties set to 10% for carbonaceous components and ions, and 20% for organic tracers. A total factor number of 4 to 7 was evaluated, and factor number 6 was selected as it provided the clearest separation of sources and minimized residuals (Fig. S2). Diagnostics of the final model showed low residuals (<10% for most variables), and the derived factor profiles matched known source characteristics. This factorization encompassed sources from fossil fuel combustion, biomass burning, the surrounding sea, primary biological emissions, biogenic secondary sources, and other fractions. The term primary biological emissions here refer to particles emitted directly from leaves, plant debris, pollen and fungal spores, following the jargon usage manner in the community. For a total of 20 base runs, 18 of them were converged and the

one with the lowest Q-value (goodness-of-fit metric) was selected. Seasonal variations in factor contributions aligned with expected patterns, such as increased biomass burning in spring and dominant fossil fuel contributions in winter, further validating the solution. The tracer method along with the PMF model was also applied to OC in an intensive Asian outflow period (January to April 2020), whose results were validated using the isotopic method based on radiocarbon analyses.

2.7 Isotopic source attribution

Radiocarbon (^{14}C) analysis was used to quantify fossil and non-fossil contributions to OC in aerosols collected from January to April 2020, to validate the PMF method for source apportionment. The rationale of this analysis is to infer information relating to WSOC and BrC.[18,,19, 51] In a similar manner, Kirillova et al. and Fang et al. observed that ^{14}C-derived fossil fractions of WSOC and OC were similar in outflow regions from East Asia,[18,19] while Miyakawa et al. reported good consistency between the carbonaceous fractions.[52] The methodology relies on distinguishing fossil-derived carbon (absent in ^{14}C) from modern biogenic sources using accelerator mass spectrometry.[52,53] Detailed analytical procedures and calculations are provided in the supporting information (Text SI1). The fractionation contributions of fossil fuel (f_{fossil}) and non-fossil fuel ($1 – f_{fossil}$) sources to the measured abundance of ^{14}C in the sample ($\Delta^{14}C$) was expressed as:

$$\Delta^{14}C\ (‰) = \Delta^{14}C_{fossil} f_{fossil} + \Delta^{14}C_{non\text{-}fossil}(1 - f_{fossil}) \qquad (2)$$

where $\Delta^{14}C_{fossil}$ is defined as –1 (as fossil carbon lacks ^{14}C) and $\Delta^{14}C_{non\text{-}fossil}$ is 181.6‰ representing biomass burning in East Asia (Text SI1 for the detailed calculations).[54-56]

TC was partitioned into fossil ($TC_{fossil} = TC \times f_{fossil}$) and non-fossil fractions ($TC_{non\text{-}fossil} = TC - TC_{fossil}$). Empirical ratios of levoglucosan to EC and OC near sources were applied to calculate biomass burning contributions (EC_{bb} and OC_{bb}).[52,57,58] Residual non-fossil OC after biomass burning contributions was attributed to biogenic sources and secondary formation (OC_{oth}).

2.8 Footprint analyses

The footprint of the Fukue observatory was simulated using the FLEXPART Lagrangian particle dispersion model (version 10.4).[59-61] which calculates the potential emission sensitivity of a receptor site by estimating BrC residence time in each 1° × 1° grid. FLEXPART was operated in backward mode to determine the source regions of air masses affecting the observatory. Meteorological data from the NCEP FNL dataset was used as input, with a 3-hour temporal resolution, a 1° × 1° spatial resolution, and 61 vertical levels. The model parameterized BrC ageing with a half-life of 1.20 days, as evaluated in this study, simplifying the combined processes of secondary production and ageing into a linear process. The BrC's half-life had a mean standard deviation of 0.26 days, however the sensitivity test indicated that the simulated residence time and the dominant footprint country did not show significant biases. Wet scavenging and dry deposition were incorporated

using the latest available scheme, where the efficiency of aerosols to serve as cloud condensation nuclei and ice nuclei were as 0.90 and 0.10, respectively.[62] The particle size was set as 0.40 μm, consistent with measurements of organic-dominated aerosol compositions at the site.[63]

For each 5-day sampling period, the footprint was simulated over a total of 10 days, including the sampling period and an additional 5 days backward in time. This approach ensured comprehensive coverage of source regions contributing to the observed BrC at Fukue. The accumulated residence time was calculated over each grid and summed these values by country. A region was defined as a "dominant footprint" if its fractional contribution exceeded the 75th percentile of its annual distribution (e.g., >26.5% for China). This method allowed us to classify air masses as China-, Korea-, Japan-, or Sea-dominated for each sampling period. A full description and thresholds are provided in SI Text ST2.

Validation of FLEXPART simulations was conducted by comparing the modeled footprints with backward trajectories generated using the HYSPLIT model. This comparison confirmed consistency between the two methods, providing confidence in the simulation results. Additionally, prior simulations of black carbon in East Asia demonstrated FLEXPART's ability to reproduce surface observations (Pearson correlation coefficient $R = 0.72$, RMSE = 0.76 μg m^{-3}), where uncertainties were primarily influenced by emission inventories. [61] In this work, the simulated footprint with high potential

emission sensitivity was passed by the backward trajectories simulated by HYSPLIT. Based on these evaluations, uncertainties in the simulated footprints affecting BrC at Fukue were deemed insignificant.

It should be noted that FLEXPART does not explicitly simulate in-plume chemical transformation, secondary BrC formation, or dynamic aerosol mixing processes. Additionally, the use of relatively coarse meteorological input (FNL, 1□ resolution) may introduce uncertainties in boundary layer height and vertical transport, especially in complex terrain or under convective conditions. In future studies, the use of chemical transport models such as WRF-Chem or GEOS-Chem may offer more detailed treatment of BrC sources, transformation, and radiative effects, including interactive chemistry and meteorology. Nonetheless, FLEXPART remains a widely used and practical tool for receptor-oriented footprint analysis, especially when combined with high-resolution observational datasets as in this study.

3. RESULTS

3.1 Seasonal variations in BrC absorption properties

3.1.1 General features. The seasonal variation of light-absorption properties of BrC aerosols was analyzed using water- (WSOC) and methanol-based (MSOC) solvents, focusing on Abs, MAC, and AAE (Fig. 1a). FLEXPART simulations revealed distinct seasonal shifts in BrC source regions, with continental influences dominating in winter and maritime influences in

summer (Fig. S3, Text SI2). Both $Abs_{365\text{-}WSOC}$ and $Abs_{365\text{-}MSOC}$ peaked in winter (0.58 ± 0.25 Mm^{-1} and 0.75 ± 0.27 Mm^{-1}, respectively) and reached their lowest values in summer (Table 1), consistent with carbonaceous aerosol component variations (Text SI3, Fig. S4). These seasonal shifts reflect the direction change of the East Asian monsoon, where the site is mainly affected by continental emissions from fossil fuel combustion and biomass burning in winter to spring,[43,51] and more influenced by local biogenic sources during summer.[64,65]

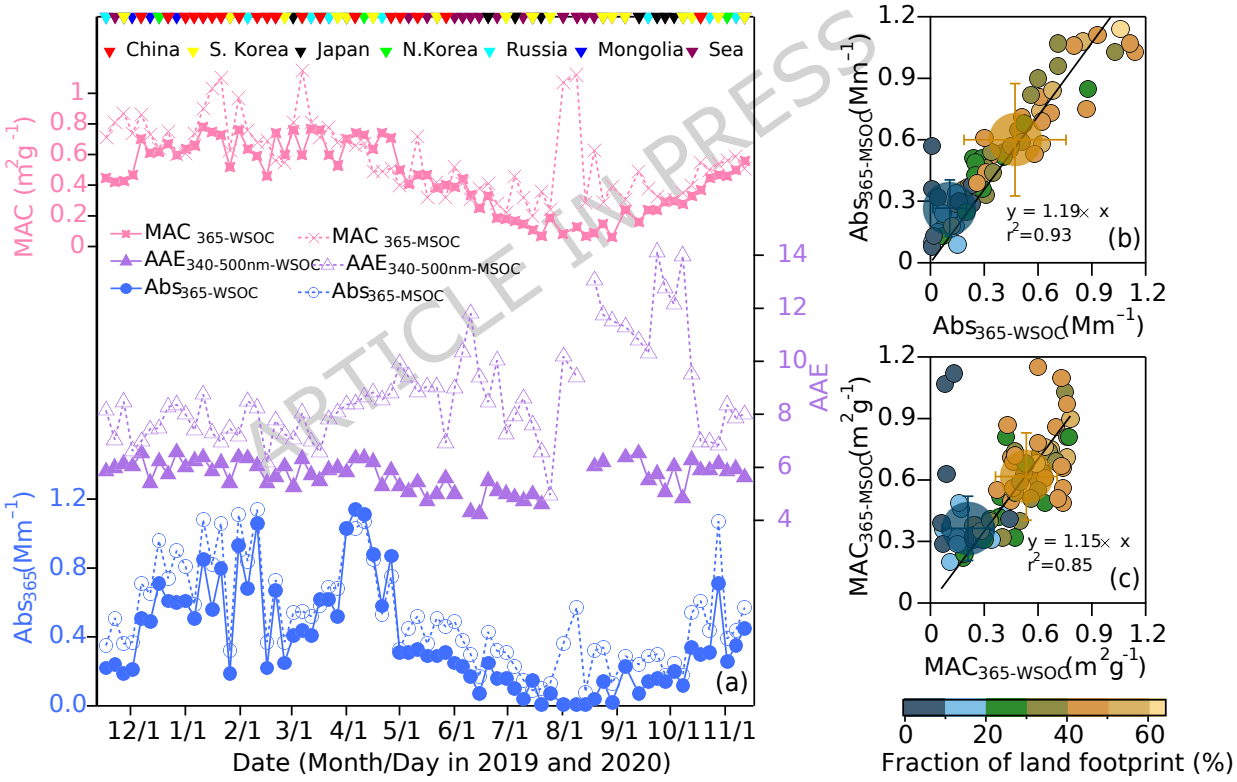

Figure 1. Light absorption properties of BrC observed at Fukue Island. (a) Temporal variations of Abs_{365}, MAC_{365}, and AAE (340–500 nm) for water and methanol extracts. Inverted triangles indicate the dominant footprint

country (FLEXPART model). (b-c) Relationships between (b) $Abs_{365\text{-}WSOC}$ and $Abs_{365\text{-}MSOC}$ and (c) $MAC_{365\text{-}WSOC}$ and $MAC_{365\text{-}MSOC}$. Mean values for land-originated footprints (fraction > 20%) and sea-originated footprints are highlighted with large brown and navy cycles, respectively, with error bars representing mean ± 1σ.

A significant reduction in Abs_{365} (from 1.06 Mm^{-1} to 0.22 Mm^{-1}) was observed in sample collected between February 13–18, 2020, continuing until early April. This period coincided with the large-scale COVID-19 lockdown in China (January 24 to March 25, 2020), which drastically curtailed transportation and industrial emissions.[32] FLEXPART simulations indicated that China was the dominant footprint for approximately half this period (Fig. 1a, Fig. S3). These findings align with reductions in BC and carbon monoxide emissions during the lockdown,[30,32] further supporting the impact of stringent emission controls.

Table 1. Seasonal and source-specific mean light absorption properties.

Season/Source	Sample size	$Abs_{365\text{-}WSOC}$ (Mm^{-1})	$Abs_{365\text{-}MSOC}$ (Mm^{-1})	$MAC_{365\text{-}WSOC}$ ($m^2\ gC^{-1}$)	$MAC_{365\text{-}MSOC}$ ($m^2\ gC^{-1}$)	$AAE_{340\text{-}500nm\text{-}WSOC}$	$AAE_{340\text{-}500nm\text{-}MSOC}$
Winter*	18	0.58 ± 0.25	0.75 ± 0.27	0.64 ± 0.09	0.75 ± 0.16	6.03 ± 0.37	7.57 ± 0.69
Spring	18	0.58 ± 0.30	0.64 ± 0.23	0.61 ± 0.14	0.61 ± 0.21	5.65 ± 0.49	8.30 ± 0.92
Summer	18	0.11 ± 0.09	0.27 ± 0.15	0.21 ± 0.14	0.56 ± 0.64	4.96 ± 0.69	8.99 ± 2.50
Autumn	14	0.26 ± 0.15	0.41 ± 0.22	0.36 ± 0.11	0.50 ± 0.17	5.87 ± 0.43	9.55 ± 2.56

Annual	71	0.38 ± 0.30	0.52 ± 0.29	0.46 ± 0.22	0.61 ± 0.36	5.68 ± 0.61	8.56 ± 1.93
Land-originated	54	0.47 ± 0.28	0.60 ± 0.27	0.53 ± 0.17	0.62 ± 0.21	5.78 ± 0.93	8.22 ± 1.62
Sea/local-originated	17	0.11 ± 0.09	0.27 ± 0.14	0.21 ± 0.14	0.36 ± 0.16	5.36 ± 2.59	9.66 ± 2.45

*: Winter is defined as December to February, with each subsequent season comprising 3 months.

The annual mean $Abs_{365\text{-}MSOC}$ was 1.35 times higher than $Abs_{365\text{-}WSOC}$ (r^2 = 0.89, $p < 0.001$, Fig. 1b, Table 1), emphasizing the contribution of water-insoluble BrC. In summer, $Abs_{365\text{-}MSOC}$ consistently exceeded $Abs_{365\text{-}WSOC}$ by a factor of 2.6, suggesting that water-insoluble BrC emitted from local vegetation or formed through secondary oxidation of volatile organic compounds was major source. Seasonal MAC_{365} trends mirrored those of Abs_{365}, with winter-spring highs and summer lows. In summer, $MAC_{365\text{-}MSOC}$ (0.56 ± 0.64 m^2 gC^{-1}) was 2.7 times higher than $MAC_{365\text{-}WSOC}$ (0.21 ± 0.14 m^2 gC^{-1}), further underscoring local contributions (e.g., 2 data points in upper-left corner of Fig. 1c). AAE did not show significant seasonal variation, however, AAE_{MSOC} (8.56 ± 1.93) was consistently higher than AAE_{WSOC} (5.68 ± 0.61), particularly during the biogenically active period from April to October (Fig. 1a, Table 1). While previous studies pointed the existence of biogenic sources in BrC emissions in populated cities, our study for the first highlighted the importance of this source in the remote outflow regions.[29,33,66,67]

3.1.2 Land- and sea-originated Abs_{365} and MAC_{365} differences. Significant differences in Abs_{365} and MAC_{365} were observed between air

masses affected by continental and maritime sources (Fig. 1b-c). Air masses predominantly originating from land (fraction of land footprint > 20%) exhibited substantially higher Abs_{365} values (e.g., $Abs_{365\text{-}WSOC}$ 0.47 ± 0.28 Mm^{-1}) compared to those from maritime and local biogenic sources ($Abs_{365\text{-}WSOC}$ 0.11 ± 0.09 Mm^{-1}). The local biogenic sources are emissions from vegetation in the island, mainly covered by laurel forest and sporadically scattered with crop land. The maritime sources could be related to emissions from biogenic production in the ocean. Similarly, $MAC_{365\text{-}WSOC}$ for land-originated air masses was 0.53 ± 0.17 m^2 gC^{-1}, more than double the value for sea-originated air masses (0.21 ± 0.14 m^2 gC^{-1}). Underscoring the significant role of source regions in shaping BrC's optical properties, these findings agreed with previous studies showing the differences of light absorption properties between those close to the emission sources in the North China Plain and those in the outflow region. [18, 19, 22-24] The pronounced distinction in Abs_{365} and MAC_{365} between land- and sea-originated air masses provide critical insights for climate modeling. We suggest that these source-specific optical properties to be incorporated into climate simulations,[6,15,16] to achieve a more accurate representation of BrC's regional and global radiative impacts.

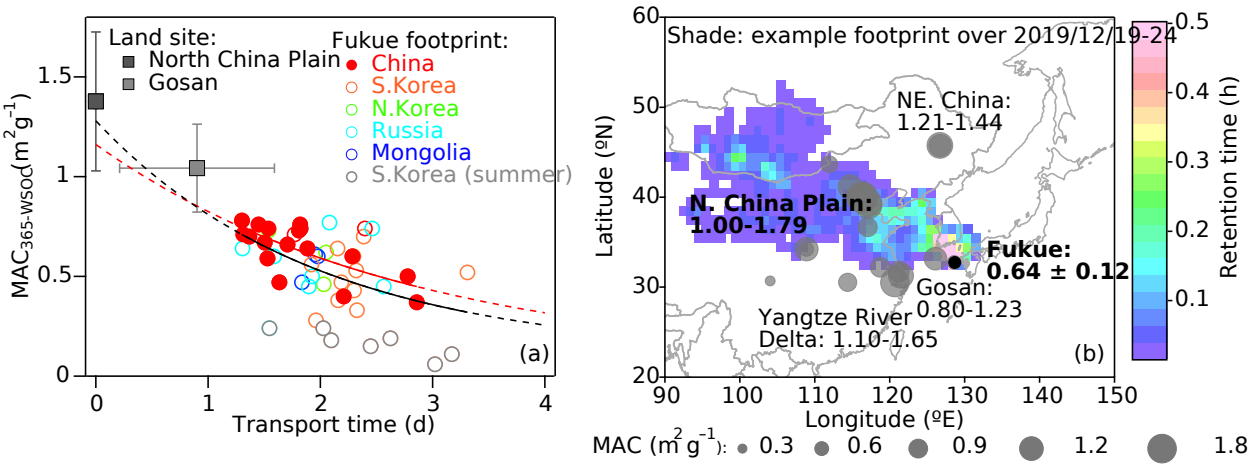

Figure 2. Photobleaching of BrC indicated by the degradation of $MAC_{365\text{-}WSOC}$ in the East Asian outflow. (a) Relationship between $MAC_{365\text{-}WSOC}$ and air mass transport time from the Asian continent to Fukue Island. Exponential fits of $MAC_{365\text{-}WSOC}$ as a function of transported time for land- (all cycles) and China-dominated (red cycles) footprints are represented by black and red lines, with dashed portions as extrapolations. (b) Representative $MAC_{365\text{-}WSOC}$ values (gray circles, $m^2\ gC^{-1}$) across the East Asia region during winter–spring outflow periods. The shaded area represents an example footprint for December 19–24, 2019. In panel (a), the fitting was conducted only based on observations at Fukue and the bars for Gosan and the North China Plain represent the standard deviations of previous studies.

3.2 Photobleaching and transport processes

The behavior of MAC at Fukue was analyzed in the context of the East Asian outflow, with a focus on the impact of continental airflow. We define photochemical degradation of BrC as the decrease in light-absorbing ability (e.g., MAC) during atmospheric transport, due to oxidative or photolytic

transformation of chromophores. The exponential decay model in Eq. (1) captures this effect, using transport time as a proxy for exposure. A clear degradation of $MAC_{365\text{-}WSOC}$ was observed with increasing transport time from the Asian continent (Fig. 2a). This trend was more pronounced for air masses dominated by Chinese footprints (red filled cycles in Fig. 2a), which were prevalent in winter to spring, with a mean $MAC_{365\text{-}WSOC}$ of 0.64 ± 0.12 $m^2\ gC^{-1}$ (n=17). This value is approximately an order of magnitude lower than those reported for the industrially intensive North China Plain, where MAC ranged from 1.00 to 1.79 $m^2\ gC^{-1}$ in winter and spring Fig. 2b, Table S1).[18,20,22-24,29,66] In other regions such as the Yangtze River Delta (1.10–1.65 $m^2\ gC^{-1}$) and Northeast China (1.21–1.44 $m^2\ gC^{-1}$),[18,20,26,68] MAC values were similar to those in the North China Plain as being closely affected by the emission sources. MAC degraded during transport, reaching 0.80–1.23 $m^2\ gC^{-1}$ at Gosan,[18,19] another site between the Asian continent and Fukue. These observations underscore the significant ageing process of BrC during atmospheric transport.

To further quantifying photobleaching, the decay rate of BrC was evaluated. For air masses dominated by Chinese footprints, the photobleaching rate was calculated as 0.57 ± 0.10 day^{-1}, corresponds to a half-life of BrC of 1.22 ± 0.26 days, and an extrapolated $MAC_{365\text{-}WSOC}$ at the China coast of 1.10 $m^2\ gC^{-1}$ (Fig. 2a, red line). This value aligns well with observations in the North China Plain (Fig. 2b, Table S1).[18,22,23,29,66] When considering all land-dominated footprints, the photobleaching rate was slightly higher at 0.62 ±

0.11 day^{-1} (half-life 1.13 ± 0.58 days), with an estimated $MAC_{365\text{-}WSOC}$ at the Asian continent of 1.18 ± 0.67 m^2 gC^{-1} (Fig. 2a, black line). These rates are higher than previous field-based estimate (0.24 ± 0.10 day^{-1}) for the North China Plain and Gosan,[18] suggesting potentially faster BrC ageing along transport pathway to Fukue. This discrepancy may reflect differences in chemical composition (e.g., higher fraction of photolabile organics), oxidant levels, aerosol liquid water content, or solar exposure during transport. Additionally, methodological differences, such as the derivation of MAC from receptor-based rather than source-proximal measurements, may contribute to the higher rates. Notably, the relatively stable MAC values reported for fresh BrC from fossil fuel combustion in the North China Plain add confidence to our back-extrapolation approach.[18,23,24,29,66] Future studies involving simultaneous observations from the continent to the remote North Pacific would provide deeper insights into the ageing processes of BrC and its variability along transport pathways.

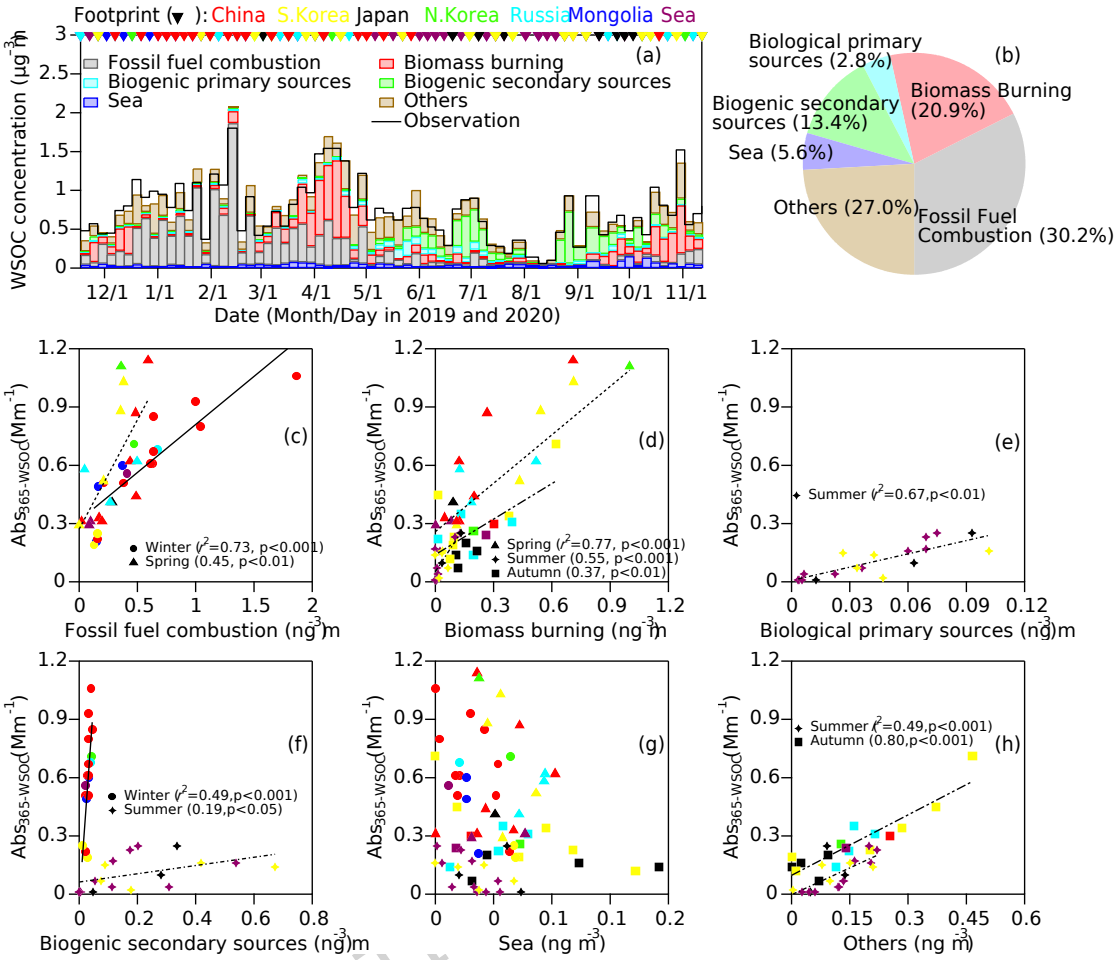

Figure 3. Source apportionment of WSOC using organic tracers and PMF model and relations with BrC absorption. (a) Temporal variation. (b) annual mean WSOC source profiles. Pearson correlations between $Abs_{365\text{-}WSOC}$ and apportioned WSOC sources from (c) fossil fuel combustion in winter and spring, (d) biomass burning in spring, summer and autumn, (e) primary biological emissions, (f) secondary biogenic sources, (g) sea emissions, and (h) other fractions. Dominant footprint regions for each sample are indicated by colored triangles in panel (a) and in the same color in panels (c-h).

3.3 Source apportionment of WSOC and relations with BrC absorption

3.3.1 General features. The source contributions of WSOC were quantified using PMF model. Among 21 organic tracers analyzed, four key groups were identified: phthalic acids (fossil fuel combustion), levoglucosan (biomass burning), glucose and mannitol (primary biological emissions), and tracers of monoterpene and isoprene (biogenic secondary formation). These tracers showed positive correlations with $Abs_{365\text{-}WSOC}$ depending on season (Fig. S5). Annual contributions to WSOC were estimated as 30.2% from fossil fuel combustion, 20.9% from biomass burning, and 16.2% from biogenic sources (Fig. 3a-b). Additionally, 27.0% of WSOC remained unresolved, likely arising from secondary formation from fossil fuel and biomass burning emissions. Nitro-aromatic compounds, a major fraction of secondary BrC, were likely formed via gas-phase photooxidation of toluene from fossil fuel combustion,[26] which in turn may contribute to WSOC. Conversely, liquid-phase reactions during biomass burning, such as the formation of imidazoles, were more prominent.[26,69] Marine contributions remained low throughout the year (5.6% on average) but showed slight increases during two typhoon events in October 2020 (Fig. 3a).

3.3.2 Seasonal variability in WSOC and related BrC sources. Sources of WSOC exhibited clear seasonal patterns (Fig. 3a). Fossil fuel combustion dominated in winter (January–February), while biomass burning peaked in

late spring (March–April). Primary biological emissions were prominent in early summer (mid-June to July), with secondary biogenic formation becoming significant from June to September. In winter and spring, $Abs_{365\text{-}WSOC}$ correlated strongly with fossil fuel combustion sources ($r^2 = 0.76$, $p < 0.001$, and $r^2 = 0.40$, $p < 0.01$, respectively; Fig. 3c), highlighting the influence of long-range transport from East Asia. Biomass burning sources were most influential in spring ($r^2 = 0.75$, $p < 0.001$; Fig. 3d), linked to open fires and domestic burning in northern China.[18,66,68,70] In summer, $Abs_{365\text{-}WSOC}$ correlated positively with both primary and secondary biogenic sources (Fig. 3e-f). These results point to local vegetation from Fukue Island as a significant BrC source in the season. In winter, $Abs_{365\text{-}WSOC}$ co-varied with secondary biogenic sources (Fig. 3f), likely driven by isoprene oxidation products (Fig. S5f). [71] While fossil fuel emissions were the primary winter source, local isoprene emissions and their subsequent oxidation may also contribute, albeit to a lesser extent, given the subtropical climate and mean air temperature of 7.6 °C in January.

3.3.3 Radiocarbon-Based Source Apportionment. The radiocarbon results confirmed a dominant contribution of fossil fuel combustion in January–February, followed by biomass burning in March–April to OC (Fig. 4a). These temporal patterns closely matched those derived from the tracer method (Fig. 4b-d, S6). Specifically, radiocarbon analysis estimated the contribution of biomass burning to OC at 19.0% (0.27 ± 0.32 μg m^{-3}), closely aligned with the tracer method estimate of 15.9% (0.22 ± 0.25 μg m^{-3}, Fig.

4b). Fossil fuel contributions were 26.0% (0.37 ± 0.14 μg m^{-3}) by the radiocarbon method, slightly lower than the 38.2% (0.53 ± 0.38 μg m^{-3}) estimated by the tracer method, likely due to the uncertainties relating to the assumptions about the non-fossil radiocarbon fraction.[18,51,52,54,72] It is worth noting that adding to absorbing fractions, non-absorbing fractions also contribute the apportioned total OC. Nevertheless, the results are inferable for WSOC related BrC sources as earlier studies showed comparable ^{14}C signatures between OC and WSOC proxies in similar receptor settings.[18,19,52] The remaining non-burning modern fraction, primarily from biogenic sources, contributed 45.9% (tracer method, 0.64 ± 0.30 μg m^{-3}) to 55.0% (radiocarbon method, 0.78 ± 0.33 μg m^{-3}) of OC. The low discrepancies (3.1%–12.2%) between methods and their consistent temporal patterns affirm the reliability of the evaluated OC source fractions.

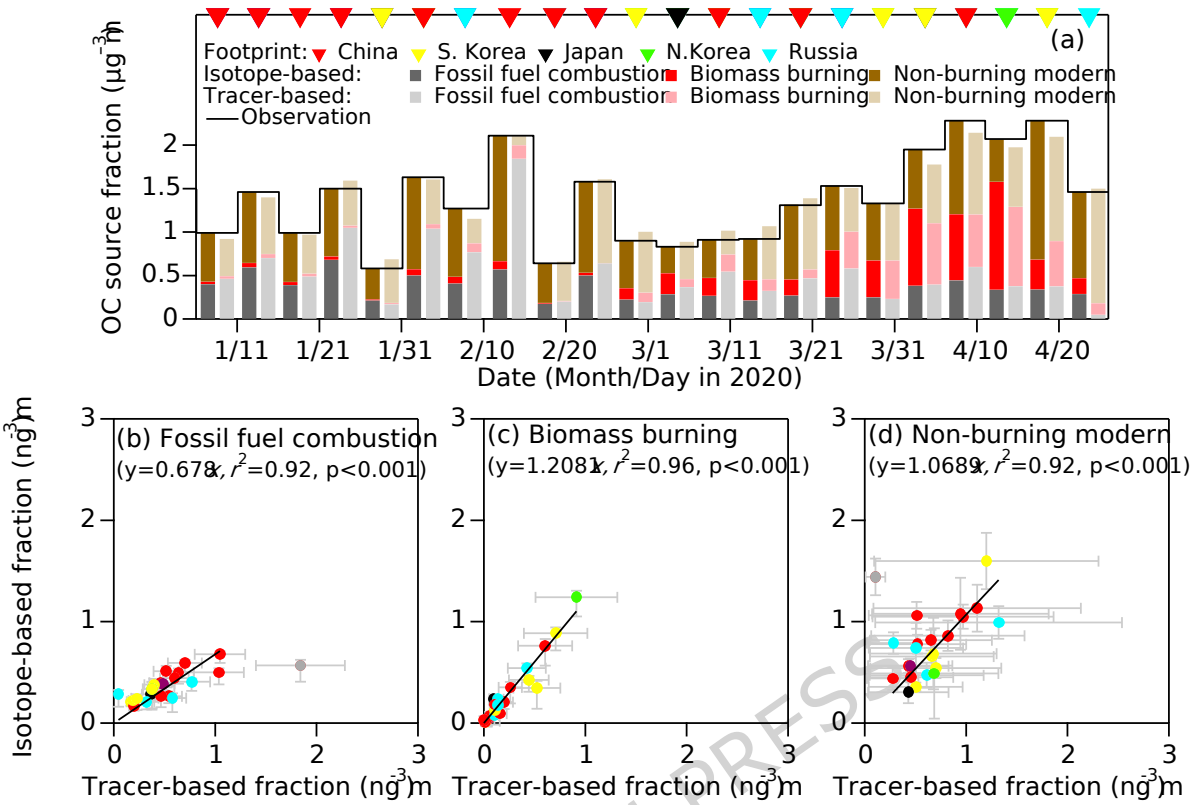

485 **Figure 4. OC sources during the intensive East Asian outflow period.** (a) Temporal profiles of OC sources, and scatter plots of tracer- and isotope-based contributions from (b) fossil fuel the combustion, (c) biomass burning and (d) other fractions. The dominant footprint region for each sample is marked with colored triangle in panel (a) and correspondingly colored data 490 points in panels (b-d). Horizontal error bars represent the 1σ standard deviation for each factor derived from the PMF model, while vertical error bars indicate the range derived using the referential fraction of $\Delta 14C_{bio}$ as reported by Fang et al. (2023).[18]

Moreover, while empirical ratios of levoglucosan to EC and OC from near-495 source biomass burning were used to estimate biomass burning

contributions, we recognize that these ratios can vary depending on fuel type, combustion conditions, and atmospheric processing. Degradation of levoglucosan during transport has been reported in prior studies, which could lead to underestimation of biomass burning contributions. However, our dataset did not indicate significant levoglucosan loss, as supported by the stable Lev/EC and Lev/OC correlations across seasons (see SI Text ST1 and Fig. S5). The combined PMF and radiocarbon results highlight the dominance of fossil fuel and biomass burning sources in winter and spring, with biogenic sources becoming more significant in summer to OC, which is inferable for BrC sources. These findings underscore the importance of incorporating source-specific BrC profiles into climate models to better represent their seasonal variability and radiative effects.

4 Discussions

4.1 Benchmark optical properties for climate models

Most climate models considered BrC as unified light absorption properties without incorporating source specific variations and atmospheric transformation such as photochemical ageing and secondary production.[73-75] As a result, large uncertainties in simulating the radiative effects of carbonaceous aerosols could been attributed to such complexity of BrC.[6,15,71] The findings from this study highlight the complex interplay of source-specific emissions, secondary formation, and photobleaching in shaping the radiative properties of BrC in the East Asian outflow. For the first time, this study

demonstrates that the MAC and Abs of BrC associated with land-originated air masses are approximately twice those of sea-originated air masses (Table 1). For climate modelers, our findings offer critical empirical input. Specifically, we provide seasonal and source-specific MAC values (e.g., 0.64 ± 0.09 m^2 gC^{-1} in winter for land-originated WSOC), which differ substantially from sea-originated air masses. Such distinctions are not represented in current global models like CAM5,[6,15] which apply uniform BrC optical properties. Inclusion of source-resolved MAC and AAE values in these models can reduce radiative forcing uncertainty, especially over East Asia.

4.2 Photobleaching and secondary formation

The atmospheric evolution of BrC involves a dynamic balance between photobleaching, which reduces its light-absorbing capacity, and secondary formation, which can partially replenish BrC during transport. Analysis of WSOC/EC ratios revealed a weak and insignificant increase with transport time from the Asian continent to Fukue (Fig. S7), suggesting limited secondary production. This is consistent with the median WSOC/EC ratio of 2.9 at Fukue, closely aligning with that of the North China Plain (2.5). This weak production, at a rate of 0.009 h^{-1}, may contribute to the unresolved BrC fraction (Fig. 3b), agreeing with previous findings.[76] Recent studies have identified key pathways for secondary BrC formation, including the photooxidation of aromatic compounds and the formation of oxygenated aromatics and imidazoles.[26,69] Incorporating these mechanisms into climate

models can improve predictions of BrC evolution during long-range transport, especially in regions like East Asia, where high precursor emissions and intense photochemical activity drive secondary BrC formation.[18,44,77,78]

4.3 Source-specific variability

The study observed a positive relationship between $AAE_{340\text{-}500nm\text{-}WSOC}$ and the $WSOC_{Biomass\ burning}$/WSOC ratio (Fig. S8), indicating that BrC from biomass burning exhibits higher light absorption potential. This finding highlights the significant role of biomass burning in shaping the optical properties of BrC,[26,66,70,79] particularly in regions affected by open fires and agricultural residue burning. With climate change projected to increase the frequency and intensity of wildfires,[35,37] biomass burning is expected to become an even more prominent source of BrC in the future. These dynamics underline the need for climate models to incorporate regionally specific BrC parameters that account for the evolving role of biomass burning in a warming world. Moreover, this study implies the importance of biogenic sources during summer and autumn, with $Abs_{365\text{-}MSOC}$ consistently exceeding $Abs_{365\text{-}WSOC}$. The findings agree with a recent work suggesting that isoprene-derived oxidation products can contribute to BrC formation.[71] The contributions of primary biogenic emissions and secondary biogenic formation should be explicitly incorporated into models, particularly in subtropical and tropical regions. Understanding how these processes interact

with changing climatic conditions, such as warming and increased atmospheric oxidant levels, is crucial for future projections.

4.4 Uncertainties and limitations

An important source of uncertainty for the sources apportionment of OC based on isotopic method arises from the reliance on empirical Lev/OC and Lev/EC ratios in estimating biomass burning contributions. These ratios are influenced by combustion conditions (e.g., flaming vs. smoldering), biomass type, and ageing during atmospheric transport. While we used representative values from multiple East Asian studies, this introduces uncertainty into the OC_{bb} and OC_{oth} estimates. Further, while our analysis suggests limited levoglucosan degradation under typical East Asian outflow conditions, variability in meteorology or oxidant levels could influence this result. A more robust approach in future studies would involve WSOC-level ^{14}C analysis to directly quantify BrC source contributions and validate molecular tracer assumptions. While the present study focused on bulk-level absorption analyses, detailed optical closure with molecular-level BrC composition was beyond the analytical scope. Future work integrating light absorption measurements with high-resolution chemical characterization, such as using the ultraperformance liquid chromatography coupled to photodiode array detector and high-resolution mass spectrometry techniques,[71] could provide deeper insights into the specific compounds responsible for BrC absorption and support improved representation in climate models.

ASSOCIATED CONTENT

Data availability Statement

The observational optical and chemical data, input for PMF analyses and isotopic analyzed results are available at https://doi.org/10.5281/zenodo.13831520. The meteorological data for FLEXPART input are available at https://rda.ucar.edu/datasets/d083002/.

Supporting Information

The Supporting Information is available. It includes further descriptions on methods for isotopic source attribution, footprint of Fukue observatory and the aerosol carbonaceous components; Table S1 about regional distribution of MAC in East Asia in winter-spring; Figure S1: Relations of BC with mean absorption coefficient at wavelengths of 700–800 nm, 695–705 nm and 795–805 nm; Figure S2: Source profiles of Positive Matrix Factorization model results; Figure S3: Footprint of Fukue Observatory simulated by FLEXPART v10.4; Figure S4: Carbonaceous components marked by country-specific footprint; Figure S5: Relations of $Abs_{365\text{-}WSOC}$ with organic tracers; Figure S6: Temporal variations of OC source contributions during the intensive East Asian outflow period; Figure S7: Relations of WSOC/EC ratio with transport time from the coast of the Asian continent to Fukue; Figure S8: Relation of $AAE_{340\text{-}500nm\text{-}WSOC}$ with $WSOC_{Biomass\ burning}$/WSOC ratio.

AUTHOR INFORMATION

Corresponding Author

*Chunmao Zhu – Research Institute for Global Change, Japan Agency for Marine-Earth Science and Technology (JAMSTEC), Yokohama 2360001, Japan; Email: chmzhu@jamstec.go.jp, Tel: +81-45-778-5365, Fax: +81-45-778-5706

Present Addresses

†Institute for Space-Earth Environmental Research, Nagoya University, Nagoya 4648601, Japan

††Space Physics Laboratory, Vikram Sarabhai Space Centre, Thiruvananthapuram 695022, India

Author Contributions

C.Z. conceived the idea. C.Z., T.M., F.T. and Y.K. conducted the observations. C.Z., T.M., B.K., D.K.D. and K.K. conducted chemical, optical and isotopic analyses. C.Z. and T.M. analyzed the data. C.Z. wrote the original manuscript along with discussions with T.M. The manuscript was written through contributions of all authors. All authors have given approval to the final version of the manuscript.

Funding Sources

This study was partly supported by the Grants-in-Aid for Scientific Research (19K20447 and 23K11401), the Arctic Challenge for Sustainability (ArCS) Project (JPMXD1300000000), ArCS II (JPMXD1420318865) and ArCS III

(JPMXD1720251001), the Steel Foundation for Environmental Protection Technology (C-40-10), and the Specified Critical Technologies Research Promotion Grants from the Cabinet Office, Government of Japan.

Notes

The authors declare no competing financial interest.

ACKNOWLEDGMENT

We thank Mr. Hidemitsu Chino for the assistance in field observation, Institute of Accelerator Analysis Ltd., Japan for the isotopic analyses and Murata Keisokuki Service Co., Ltd., Japan for a part of optical and chemical analyses.

REFERENCES

(1) Hecobian, A.; Zhang, X.; Zheng, M.; Frank, N.; Edgerton, E. S.; Weber, R. J. Water-Soluble Organic Aerosol material and the light-absorption characteristics of aqueous extracts measured over the Southeastern United States. *Atmos Chem Phys* **2010**, *10* (13), 5965–5977. DOI: 10.5194/acp-10-5965-2010.

(2) Laskin, A.; Laskin, J.; Nizkorodov, S. A. Chemistry of Atmospheric Brown Carbon. *Chem Rev* **2015**, *115* (10), 4335–4382. DOI: 10.1021/cr5006167.

(3) Chakrabarty, R. K.; Shetty, N. J.; Thind, A. S.; Beeler, P.; Sumlin, B. J.; Zhang, C.; Liu, P.; Idrobo, J. C.; Adachi, K.; Wagner, N. L.; et al. Shortwave absorption by wildfire smoke dominated by dark brown carbon. *Nat Geosci* **2023**, *16* (8), 683–688. DOI: 10.1038/s41561-023-01237-9.

(4) Alexander, D. T. L.; Crozier, P. A.; Anderson, J. R. Brown Carbon Spheres in East Asian Outflow and Their Optical Properties. *Science* **2008**, *321* (5890), 833–836. DOI: 10.1126/science.1155296.

(5) Zeng, L. H.; Zhang, A. X.; Wang, Y. H.; Wagner, N. L.; Katich, J. M.; Schwarz, J. P.; Schill, G. P.; Brock, C.; Froyd, K. D.; Murphy, D. M.; et al. Global Measurements of Brown Carbon and Estimated Direct Radiative Effects. *Geophys Res Lett* **2020**, *47* (13), e2020GL088747. DOI: 10.1029/2020GL088747.

(6) Zhang, A. X.; Wang, Y. H.; Zhang, Y. Z.; Weber, R. J.; Song, Y. J.; Ke, Z. M.; Zou, Y. F. Modeling the global radiative effect of brown carbon: a potentially larger heating source in the tropical free troposphere than black carbon. *Atmos Chem Phys* **2020**, *20* (4), 1901–1920. DOI: 10.5194/acp-20-1901-2020.
(7) Zhang, Y. Z.; Forrister, H.; Liu, J. M.; Dibb, J.; Anderson, B.; Schwarz, J. P.; Perring, A. E.; Jimenez, J. L.; Campuzano-Jost, P.; Wang, Y. H.; et al. Top-of-atmosphere radiative forcing affected by brown carbon in the upper troposphere. *Nat Geosci* **2017**, *10* (7), 486–489. DOI: 10.1038/Ngeo2960.
(8) Cheng, Y.; Chow, J. C.; Watson, J. G.; Zhou, J.; Liu, S.; Cao, J. Decreasing concentrations of carbonaceous aerosols in China from 2003 to 2013. *Sci Rep-Uk* **2021**, *11* (1), 5352. DOI: 10.1038/s41598-021-84429-w.
(9) Kalita, G.; Kunchala, R. K.; Fadnavis, S.; Kaskaoutis, D. G. Long term variability of carbonaceous aerosols over Southeast Asia via reanalysis: Association with changes in vegetation cover and biomass burning. *Atmospheric research* **2020**, *245*, 105064. DOI: 10.1016/j.atmosres.2020.105064.
(10) Yttri, K. E.; Canonaco, F.; Eckhardt, S.; Evangeliou, N.; Fiebig, M.; Gundersen, H.; Hjellbrekke, A.-G.; Lund Myhre, C.; Platt, S. M.; Prévôt, A. S. Trends, composition, and sources of carbonaceous aerosol at the Birkenes Observatory, northern Europe, 2001–2018. *Atmos Chem Phys* **2021**, *21* (9), 7149–7170. DOI: 10.5194/acp-21-7149-2021.
(11) Zhou, R.; Yan, C.; Yang, Q.; Niu, H.; Liu, J.; Xue, F.; Chen, B.; Zhou, T.; Chen, H.; Liu, J. Characteristics of wintertime carbonaceous aerosols in two typical cities in Beijing-Tianjin-Hebei region, China: Insights from multiyear measurements. *Environmental Research* **2023**, *216*, 114469. DOI: 10.1016/j.envres.2022.114469.
(12) Kaskaoutis, D. G.; Liakakou, E.; Grivas, G.; Gerasopoulos, E.; Mihalopoulos, N.; Alastuey, A.; Dulac, F.; Dumka, U. C.; Pandolfi, M.; Pikridas, M. Interannual variability and long-term trends of aerosols above the Mediterranean. In *Atmospheric Chemistry in the Mediterranean Region: Volume 1-Background Information and Pollutant Distribution*, Springer, 2023; pp 357–390.
(13) Li, J.; Carlson, B. E.; Yung, Y. L.; Lv, D.; Hansen, J.; Penner, J. E.; Liao, H.; Ramaswamy, V.; Kahn, R. A.; Zhang, P.; et al. Scattering and absorbing aerosols in the climate system. *Nature Reviews Earth & Environment* **2022**, *3* (6), 363–379. DOI: 10.1038/s43017-022-00296-7.
(14) Masson-Delmotte, V.; Zhai, P.; Pirani, A.; Connors, S.; Péan, C.; Berger, S.; Caud, N.; Chen, Y.; Goldfarb, L.; Gomis, M. Contribution of working group I to the sixth assessment report of the intergovernmental panel on climate change. *Climate change 2021: the physical science basis* **2021**.
(15) Brown, H.; Liu, X.; Feng, Y.; Jiang, Y.; Wu, M.; Lu, Z.; Wu, C.; Murphy, S.; Pokhrel, R. Radiative effect and climate impacts of brown carbon with the Community Atmosphere Model (CAM5). *Atmos Chem Phys* **2018**, *18* (24), 17745–17768. DOI: 10.5194/acp-18-17745-2018.

(16) Brown, H.; Liu, X.; Pokhrel, R.; Murphy, S.; Lu, Z.; Saleh, R.; Mielonen, T.; Kokkola, H.; Bergman, T.; Myhre, G.; et al. Biomass burning aerosols in most climate models are too absorbing. *Nat Commun* **2021**, *12* (1), 277. DOI: 10.1038/s41467-020-20482-9.
(17) Liu, D. T.; He, C. L.; Schwarz, J. P.; Wang, X. Lifecycle of light-absorbing carbonaceous aerosols in the atmosphere. *Npj Clim Atmos Sci* **2020**, *3* (1), 40. DOI: 10.1038/s41612-020-00145-8.
(18) Fang, W.; Andersson, A.; Lee, M.; Zheng, M.; Du, K.; Kim, S.-W.; Holmstrand, H.; Gustafsson, Ö. Combined influences of sources and atmospheric bleaching on light absorption of water-soluble brown carbon aerosols. *Npj Clim Atmos Sci* **2023**, *6* (1), 104. DOI: 10.1038/s41612-023-00438-8.
(19) Kirillova, E. N.; Andersson, A.; Han, J.; Lee, M.; Gustafsson, Ö. Sources and light absorption of water-soluble organic carbon aerosols in the outflow from northern China. *Atmos. Chem. Phys.* **2014**, *14* (3), 1413–1422. DOI: 10.5194/acp-14-1413-2014.
(20) Wang, D.; Shen, Z.; Zhang, Q.; Lei, Y.; Zhang, T.; Huang, S.; Sun, J.; Xu, H.; Cao, J. Winter brown carbon over six of China's megacities: light absorption, molecular characterization, and improved source apportionment revealed by multilayer perceptron neural network. *Atmos. Chem. Phys.* **2022**, *22* (22), 14893–14904. DOI: 10.5194/acp-22-14893-2022.
(21) Zhong, M.; Xu, J.; Wang, H.; Gao, L.; Zhu, H.; Zhai, L.; Zhang, X.; Zhao, W. Characterizing water-soluble brown carbon in fine particles in four typical cities in northwestern China during wintertime: integrating optical properties with chemical processes. *Atmos Chem Phys* **2023**, *23* (19), 12609–12630.
(22) Yan, C.; Zheng, M.; Sullivan, A. P.; Bosch, C.; Desyaterik, Y.; Andersson, A.; Li, X.; Guo, X.; Zhou, T.; Gustafsson, Ö.; et al. Chemical characteristics and light-absorbing property of water-soluble organic carbon in Beijing: Biomass burning contributions. *Atmos Environ* **2015**, *121*, 4–12. DOI: 10.1016/j.atmosenv.2015.05.005.
(23) Du, Z.; He, K.; Cheng, Y.; Duan, F.; Ma, Y.; Liu, J.; Zhang, X.; Zheng, M.; Weber, R. A yearlong study of water-soluble organic carbon in Beijing II: Light absorption properties. *Atmos Environ* **2014**, *89*, 235–241. DOI: 10.1016/j.atmosenv.2014.02.022.
(24) Cheng, Y.; He, K. B.; Zheng, M.; Duan, F. K.; Du, Z. Y.; Ma, Y. L.; Tan, J. H.; Yang, F. M.; Liu, J. M.; Zhang, X. L.; et al. Mass absorption efficiency of elemental carbon and water-soluble organic carbon in Beijing, China. *Atmos. Chem. Phys.* **2011**, *11* (22), 11497–11510. DOI: 10.5194/acp-11-11497-2011.
(25) Lei, Y.; Zhang, K.; Lu, Y.; Qin, Y.; Li, L.; Li, J.; Liu, X.; Wu, C.; Zhang, S.; Chen, Y.; et al. Characterization of water−soluble brown carbon in atmospheric fine particles over Xi'an, China: Implication of aqueous brown carbon formation from biomass burning. *Sci Total Environ* **2023**, *881*, 163442. DOI: 10.1016/j.scitotenv.2023.163442.

(26) Liu, X.; Wang, H.; Wang, F.; Lv, S.; Wu, C.; Zhao, Y.; Zhang, S.; Liu, S.; Xu, X.; Lei, Y.; et al. Secondary Formation of Atmospheric Brown Carbon in China Haze: Implication for an Enhancing Role of Ammonia. *Environ Sci Technol* **2023**, *57* (30), 11163–11172. DOI: 10.1021/acs.est.3c03948.
(27) Forrister, H.; Liu, J.; Scheuer, E.; Dibb, J.; Ziemba, L.; Thornhill, K. L.; Anderson, B.; Diskin, G.; Perring, A. E.; Schwarz, J. P.; et al. Evolution of brown carbon in wildfire plumes. *Geophys Res Lett* **2015**, *42* (11), 4623–4630. DOI: 10.1002/2015gl063897.
(28) Li, Q.; Liu, D.; Jiang, X.; Tian, P.; Wu, Y.; Li, S.; Hu, K.; Liu, Q.; Huang, M.; Li, R.; et al. Concurrent photochemical whitening and darkening of ambient brown carbon. *Atmos. Chem. Phys.* **2023**, *23* (16), 9439–9453. DOI: 10.5194/acp-23-9439-2023.
(29) Wen, H.; Zhou, Y.; Xu, X.; Wang, T.; Chen, Q.; Chen, Q.; Li, W.; Wang, Z.; Huang, Z.; Zhou, T.; et al. Water-soluble brown carbon in atmospheric aerosols along the transport pathway of Asian dust: Optical properties, chemical compositions, and potential sources. *Sci Total Environ* **2021**, *789*, 147971. DOI: 10.1016/j.scitotenv.2021.147971.
(30) Kanaya, Y.; Yamaji, K.; Miyakawa, T.; Taketani, F.; Zhu, C.; Choi, Y.; Komazaki, Y.; Ikeda, K.; Kondo, Y.; Klimont, Z. Rapid reduction in black carbon emissions from China: evidence from 2009-2019 observations on Fukue Island, Japan. *Atmos Chem Phys* **2020**, *20* (11), 6339–6356. DOI: 10.5194/acp-20-6339-2020.
(31) Zheng, B.; Tong, D.; Li, M.; Liu, F.; Hong, C. P.; Geng, G. N.; Li, H. Y.; Li, X.; Peng, L. Q.; Qi, J.; et al. Trends in China's anthropogenic emissions since 2010 as the consequence of clean air actions. *Atmos Chem Phys* **2018**, *18* (19), 14095–14111. DOI: 10.5194/acp-18-14095-2018.
(32) Chen, Q.; Miao, R.; Geng, G.; Shrivastava, M.; Dao, X.; Xu, B.; Sun, J.; Zhang, X.; Liu, M.; Tang, G.; et al. Widespread 2013-2020 decreases and reduction challenges of organic aerosol in China. *Nat Commun* **2024**, *15* (1), 4465. DOI: 10.1038/s41467-024-48902-0 From NLM PubMed-not-MEDLINE.
(33) Updyke, K. M.; Nguyen, T. B.; Nizkorodov, S. A. Formation of brown carbon via reactions of ammonia with secondary organic aerosols from biogenic and anthropogenic precursors. *Atmos Environ* **2012**, *63*, 22–31. DOI: 10.1016/j.atmosenv.2012.09.012.
(34) Nguyen, T. B.; Laskin, A.; Laskin, J.; Nizkorodov, S. A. Brown carbon formation from ketoaldehydes of biogenic monoterpenes. *Faraday Discuss* **2013**, *165*, 473–494. DOI: 10.1039/c3fd00036b.
(35) Veira, A.; Lasslop, G.; Kloster, S. Wildfires in a warmer climate: Emission fluxes, emission heights, and black carbon concentrations in 2090-2099. *J Geophys Res-Atmos* **2016**, *121* (7), 3195–3223. DOI: 10.1002/2015jd024142.
(36) Zhu, C.; Kanaya, Y.; Yoshikawa-Inoue, H.; Irino, T.; Seki, O.; Tohjima, Y. Sources of atmospheric black carbon and related carbonaceous components at Rishiri Island, Japan: The roles of Siberian wildfires and of crop residue

burning in China. *Environ Pollut* **2019**, *247*, 55–63. DOI: 10.1016/j.envpol.2019.01.003.
(37) Pérez-Invernón, F. J.; Gordillo-Vázquez, F. J.; Huntrieser, H.; Jöckel, P. Variation of lightning-ignited wildfire patterns under climate change. *Nat Commun* **2023**, *14* (1), 739. DOI: 10.1038/s41467-023-36500-5.
(38) Bai, Z.; Zhang, L.; Cheng, Y.; Zhang, W.; Mao, J.; Chen, H.; Li, L.; Wang, L.; Chen, J. Water/Methanol-Insoluble Brown Carbon Can Dominate Aerosol-Enhanced Light Absorption in Port Cities. *Environ Sci Technol* **2020**, *54* (23), 14889–14898. DOI: 10.1021/acs.est.0c03844.
(39) Birch, M. E.; Cary, R. A. Elemental carbon-based method for occupational monitoring of particulate diesel exhaust: methodology and exposure issues. *Analyst* **1996**, *121* (9), 1183–1190, 10.1039/AN9962101183. DOI: 10.1039/AN9962101183.
(40) Cheng, Y.; He, K.-b.; Du, Z.-y.; Engling, G.; Liu, J.-m.; Ma, Y.-l.; Zheng, M.; Weber, R. J. The characteristics of brown carbon aerosol during winter in Beijing. *Atmos Environ* **2016**, *127*, 355–364. DOI: 10.1016/j.atmosenv.2015.12.035.
(41) Xie, X. C.; Chen, Y. F.; Nie, D. Y.; Liu, Y.; Liu, Y.; Lei, R. Y.; Zhao, X. Y.; Li, H. W.; Ge, X. L. Light-absorbing and fluorescent properties of atmospheric brown carbon: A case study in Nanjing, China. *Chemosphere* **2020**, *251*, 126350. DOI: 10.1016/j.chemosphere.2020.126350.
(42) Phillips, S. M.; Smith, G. D. Spectroscopic comparison of water- and methanol-soluble brown carbon particulate matter. *Aerosol Sci Tech* **2017**, *51* (9), 1113–1121. DOI: 10.1080/02786826.2017.1334109.
(43) Zhu, C.; Miyakawa, T.; Irie, H.; Choi, Y.; Taketani, F.; Kanaya, Y. Light-absorption properties of brown carbon aerosols in the Asian outflow: Implications of a combination of filter and ground remote-sensing observations at Fukue Island, Japan. *Sci Total Environ* **2021**, *797*, 149155. DOI: https://doi.org/10.1016/j.scitotenv.2021.149155.
(44) Dasari, S.; Andersson, A.; Bikkina, S.; Holmstrand, H.; Budhavant, K.; Satheesh, S.; Asmi, E.; Kesti, J.; Backman, J.; Salam, A.; et al. Photochemical degradation affects the light absorption of water-soluble brown carbon in the South Asian outflow. *Sci Adv* **2019**, *5* (1), eaau8066. DOI: doi:10.1126/sciadv.aau8066.
(45) Stein, A. F.; Draxler, R. R.; Rolph, G. D.; Stunder, B. J. B.; Cohen, M. D.; Ngan, F. NOAA's HYSPLIT Atmospheric Transport and Dispersion Modeling System. *B Am Meteorol Soc* **2015**, *96* (12), 2059–2077. DOI: https://doi.org/10.1175/BAMS-D-14-00110.1.
(46) Simoneit, B. R. T.; Elias, V. O.; Kobayashi, M.; Kawamura, K.; Rushdi, A. I.; Medeiros, P. M.; Rogge, W. F.; Didyk, B. M. Sugars Dominant Water-Soluble Organic Compounds in Soils and Characterization as Tracers in Atmospheric Particulate Matter. *Environ Sci Technol* **2004**, *38* (22), 5939–5949. DOI: 10.1021/es0403099.
(47) Zhu, C.; Kawamura, K.; Kunwar, B. Effect of biomass burning over the western North Pacific Rim: wintertime maxima of anhydrosugars in ambient

aerosols from Okinawa. *Atmos. Chem. Phys.* **2015**, *15* (4), 1959–1973. DOI: 10.5194/acp-15-1959-2015.
(48) Fu, P.; Kawamura, K.; Okuzawa, K.; Aggarwal, S. G.; Wang, G.; Kanaya, Y.; Wang, Z. Organic molecular compositions and temporal variations of summertime mountain aerosols over Mt. Tai, North China Plain. *Journal of Geophysical Research: Atmospheres* **2008**, *113*, D19107. DOI: https://doi.org/10.1029/2008JD009900.
(49) Zhu, C.; Kawamura, K.; Fukuda, Y.; Mochida, M.; Iwamoto, Y. Fungal spores overwhelm biogenic organic aerosols in a midlatitudinal forest. *Atmos. Chem. Phys.* **2016**, *16* (11), 7497–7506. DOI: 10.5194/acp-16-7497-2016.
(50) Brown, S. G.; Eberly, S.; Paatero, P.; Norris, G. A. Methods for estimating uncertainty in PMF solutions: Examples with ambient air and water quality data and guidance on reporting PMF results. *Sci Total Environ* **2015**, *518-519*, 626–635. DOI: https://doi.org/10.1016/j.scitotenv.2015.01.022.
(51) Jiang, H.; Li, J.; Sun, R.; Liu, G.; Tian, C.; Tang, J.; Cheng, Z.; Zhu, S.; Zhong, G.; Ding, X.; et al. Determining the Sources and Transport of Brown Carbon Using Radionuclide Tracers and Modeling. *Journal of Geophysical Research: Atmospheres* **2021**, *126* (9), e2021JD034616. DOI: https://doi.org/10.1029/2021JD034616.
(52) Miyakawa, T.; Komazaki, Y.; Zhu, C.; Taketani, F.; Pan, X.; Wang, Z.; Kanaya, Y. Characterization of carbonaceous aerosols in Asian outflow in the spring of 2015: Importance of non-fossil fuel sources. *Atmos Environ* **2019**, *214*, 116858. DOI: https://doi.org/10.1016/j.atmosenv.2019.116858.
(53) Miyakawa, T.; Kanaya, Y.; Komazaki, Y.; Miyoshi, T.; Nara, H.; Takami, A.; Moteki, N.; Koike, M.; Kondo, Y. Emission Regulations Altered the Concentrations, Origin, and Formation of Carbonaceous Aerosols in the Tokyo Metropolitan Area. *Aerosol Air Qual Res* **2016**, *16* (7), 1603–1614. DOI: 10.4209/aaqr.2015.11.0624.
(54) Gustafsson, Ö.; Kruså, M.; Zencak, Z.; Sheesley, R. J.; Granat, L.; Engström, E.; Praveen, P. S.; Rao, P. S. P.; Leck, C.; Rodhe, H. Brown Clouds over South Asia: Biomass or Fossil Fuel Combustion? *Science* **2009**, *323* (5913), 495–498. DOI: doi:10.1126/science.1164857.
(55) Shen, G.; Xiong, R.; Tian, Y.; Luo, Z.; Jiangtulu, B.; Meng, W.; Du, W.; Meng, J.; Chen, Y.; Xue, B.; et al. Substantial transition to clean household energy mix in rural China. *National Science Review* **2022**, *9* (7), nwac050. DOI: 10.1093/nsr/nwac050 (acccessed 9/20/2024).
(56) Du, W.; Wang, J.; Feng, Y.; Duan, W.; Wang, Z.; Chen, Y.; Zhang, P.; Pan, B. Biomass as residential energy in China: Current status and future perspectives. *Renewable and Sustainable Energy Reviews* **2023**, *186*, 113657. DOI: https://doi.org/10.1016/j.rser.2023.113657.
(57) Mazzoleni, L. R.; Zielinska, B.; Moosmüller, H. Emissions of Levoglucosan, Methoxy Phenols, and Organic Acids from Prescribed Burns, Laboratory Combustion of Wildland Fuels, and Residential Wood

Combustion. *Environ Sci Technol* **2007**, *41* (7), 2115–2122. DOI: 10.1021/es061702c.
(58) Zhang, Y.-x.; Shao, M.; Zhang, Y.-h.; Zeng, L.-m.; He, L.-y.; Zhu, B.; Wei, Y.-j.; Zhu, X.-l. Source profiles of particulate organic matters emitted from cereal straw burnings. *Journal of Environmental Sciences* **2007**, *19* (2), 167–175. DOI: https://doi.org/10.1016/S1001-0742(07)60027-8.
(59) Pisso, I.; Sollum, E.; Grythe, H.; Kristiansen, N. I.; Cassiani, M.; Eckhardt, S.; Arnold, D.; Morton, D.; Thompson, R. L.; Groot Zwaaftink, C. D.; et al. The Lagrangian particle dispersion model FLEXPART version 10.4. *Geosci Model Dev* **2019**, *12* (12), 4955–4997. DOI: 10.5194/gmd-12-4955-2019.
(60) Stohl, A.; Hittenberger, M.; Wotawa, G. Validation of the Lagrangian particle dispersion model FLEXPART against large-scale tracer experiment data. *Atmos Environ* **1998**, *32* (24), 4245–4264. DOI: 10.1016/S1352-2310(98)00184-8.
(61) Fang, W.; Evangeliou, N.; Eckhardt, S.; Xing, J.; Zhang, H.; Xiao, H.; Zhao, M.; Kim, S.-W. Increased contribution of biomass burning to haze events in Shanghai since China's clean air actions. Communications Earth & Environment 2023, 4 (1), 310. DOI: 10.1038/s43247-023-00979-z.
(62) Grythe, H.; Kristiansen, N. I.; Groot Zwaaftink, C. D.; Eckhardt, S.; Ström, J.; Tunved, P.; Krejci, R.; Stohl, A. A new aerosol wet removal scheme for the Lagrangian particle model FLEXPART v10. *Geosci Model Dev* **2017**, *10* (4), 1447–1466. DOI: 10.5194/gmd-10-1447-2017.
(63) Takami, A.; Miyoshi, T.; Shimono, A.; Hatakeyama, S. Chemical composition of fine aerosol measured by AMS at Fukue Island, Japan during APEX period. *Atmos Environ* **2005**, *39* (27), 4913–4924. DOI: 10.1016/j.atmosenv.2005.04.038.
(64) Zhu, C.; Kawamura, K.; Fu, P. Seasonal variations of biogenic secondary organic aerosol tracers in Cape Hedo, Okinawa. *Atmos Environ* **2016**, *130*, 113-119. DOI: 10.1016/j.atmosenv.2015.08.069.
(65) Zhu, C.; Kawamura, K.; Kunwar, B. Organic tracers of primary biological aerosol particles at subtropical Okinawa Island in the western North Pacific Rim. *Journal of Geophysical Research: Atmospheres* **2015**, *120* (11), 5504-5523. DOI: 10.1002/2015jd023611.
(66) Deng, J.; Ma, H.; Wang, X.; Zhong, S.; Zhang, Z.; Zhu, J.; Fan, Y.; Hu, W.; Wu, L.; Li, X.; et al. Measurement report: Optical properties and sources of water-soluble brown carbon in Tianjin, North China – insights from organic molecular compositions. *Atmos. Chem. Phys.* **2022**, *22* (10), 6449–6470. DOI: 10.5194/acp-22-6449-2022.
(67) Chen, Q. C.; Miyazaki, Y.; Kawamura, K.; Matsumoto, K.; Coburn, S.; Volkamer, R.; Iwamoto, Y.; Kagami, S.; Deng, Y. G.; Ogawa, S.; et al. Characterization of Chromophoric Water-Soluble Organic Matter in Urban, Forest, and Marine Aerosols by HR-ToF-AMS Analysis and Excitation Emission Matrix Spectroscopy. *Environ Sci Technol* **2016**, *50* (19), 10351–10360. DOI: 10.1021/acs.est.6b01643.

(68) Cheng, Y.; Cao, X.-b.; Liu, J.-m.; Yu, Q.-q.; Wang, P.; Yan, C.-q.; Du, Z.-y.; Liang, L.-l.; Zhang, Q.; He, K.-b. Primary nature of brown carbon absorption in a frigid atmosphere with strong haze chemistry. *Environmental Research* **2022**, *204*, 112324. DOI: 10.1016/j.envres.2021.112324.
(69) Yang, L.; Huang, R.-J.; Shen, J.; Wang, T.; Gong, Y.; Yuan, W.; Liu, Y.; Huang, H.; You, Q.; Huang, D. D.; et al. New Insights into the Brown Carbon Chromophores and Formation Pathways for Aqueous Reactions of α-Dicarbonyls with Amines and Ammonium. *Environ Sci Technol* **2023**, *57* (33), 12351-12361. DOI: 10.1021/acs.est.3c04133.
(70) Dong, Z.; Pavuluri, C. M.; Li, P.; Xu, Z.; Deng, J.; Zhao, X.; Zhao, X.; Fu, P.; Liu, C. Q. Measurement report: Optical characterization, seasonality, and sources of brown carbon in fine aerosols from Tianjin, North China: year-round observations. *Atmos. Chem. Phys.* **2024**, *24* (10), 5887–5905. DOI: 10.5194/acp-24-5887-2024.
(71) Laskin, A.; West, C. P.; Hettiyadura, A. P. S. Molecular insights into the composition, sources, and aging of atmospheric brown carbon. *Chemical Society Reviews* **2025**, 10.1039/D3CS00609C. DOI: 10.1039/D3CS00609C.
(72) Sun, X.; Hu, M.; Guo, S.; Liu, K.; Zhou, L. 14C-Based source assessment of carbonaceous aerosols at a rural site. *Atmos Environ* **2012**, *50*, 36–40. DOI: https://doi.org/10.1016/j.atmosenv.2012.01.008.
(73) Jo, D. S.; Park, R. J.; Lee, S.; Kim, S. W.; Zhang, X. A global simulation of brown carbon: implications for photochemistry and direct radiative effect. *Atmos. Chem. Phys.* **2016**, *16* (5), 3413-3432. DOI: 10.5194/acp-16-3413-2016.
(74) Saleh, R.; Marks, M.; Heo, J.; Adams, P. J.; Donahue, N. M.; Robinson, A. L. Contribution of brown carbon and lensing to the direct radiative effect of carbonaceous aerosols from biomass and biofuel burning emissions. *Journal of Geophysical Research: Atmospheres* **2015**, *120* (19), 10,285-210,296. DOI: https://doi.org/10.1002/2015JD023697.
(75) Xu, L.; Lin, G.; Liu, X.; Wu, C.; Wu, Y.; Lou, S. Constraining light absorption of brown carbon in China and implications for aerosol direct radiative effect. *Geophys Res Lett* **2024**, *51* (16), e2024GL109861.
(76) Sahu, L. K.; Kondo, Y.; Miyazaki, Y.; Kuwata, M.; Koike, M.; Takegawa, N.; Tanimoto, H.; Matsueda, H.; Yoon, S. C.; Kim, Y. J. Anthropogenic aerosols observed in Asian continental outflow at Jeju Island, Korea, in spring 2005. *Journal of Geophysical Research: Atmospheres* **2009**, *114* (D3). DOI: https://doi.org/10.1029/2008JD010306.
(77) Saleh, R.; Hennigan, C. J.; McMeeking, G. R.; Chuang, W. K.; Robinson, E. S.; Coe, H.; Donahue, N. M.; Robinson, A. L. Absorptivity of brown carbon in fresh and photo-chemically aged biomass-burning emissions. *Atmos Chem Phys* **2013**, *13* (15), 7683–7693. DOI: 10.5194/acp-13-7683-2013.
(78) Ni, H.; Huang, R.-J.; Pieber, S. M.; Corbin, J. C.; Stefenelli, G.; Pospisilova, V.; Klein, F.; Gysel-Beer, M.; Yang, L.; Baltensperger, U.; et al. Brown Carbon in Primary and Aged Coal Combustion Emission. *Environ Sci Technol* **2021**, *55* (9), 5701–5710. DOI: 10.1021/acs.est.0c08084.

(79) Basnet, S.; Hartikainen, A.; Virkkula, A.; Yli-Pirilä, P.; Kortelainen, M.; Suhonen, H.; Kilpeläinen, L.; Ihalainen, M.; Väätäinen, S.; Louhisalmi, J.; et al. Contribution of brown carbon to light absorption in emissions of European residential biomass combustion appliances. *Atmos. Chem. Phys.* **2024**, *24* (5), 3197–3215. DOI: 10.5194/acp-24-3197-2024.